Elucidating structure–property relationships in Cd(II) coordination polymers for charge transport and Schottky device fabrication

Ersad Hossain,[a,b] Ramjan Sk,[c] Sayantan Sil,[d] Samit Pramanik,[e] Partha Pratim Ray,*[b] Joaquin Ortega-Castro, [f] Antonio Frontera,[f] Mohammad Hedayetullah Mir,*[a] and Subrata Mukhopadhyay,*[b]

[a]*Department of Chemistry, Aliah University, New Town, Kolkata 700 160, India*

[b]*Department of Chemistry, Jadavpur University, Kolkata 700032, India*

[c]*Department of Physics, Jadavpur University, Kolkata 700032, India*

[d]*Department of Physics, Institute of Engineering and management, University of Engineering and Management, Kolkata, University Area, Action Area III, B/5, New Town, Kolkata 700160, India*

[e]*Department of basic science and humanities, Alipurduar Government Engineering and Management College, Bakla, Alipurduar 736206, India*

[f]*Department of Chemistry, Universitat de les Illes Balears, Crta de Valldemossa km 7.5, 07122 Palma de Mallorca (Baleares), Spain.*

Supporting Information

Experimental section

Materials and methods

The chemicals were utilized exactly as they were received from various chemical companies. For the crystallization procedure, high purity cadmium(II) nitrate tetrahydrate [$Cd(NO_3)_2 \cdot 4H_2O$], 2,5-dichloroterephthalic acid (H_2DCTP) and 2,5-dibromoterephthalic acid (H_2DBTP) were utilized. All other compounds and solvents were used as AR grade and were used in this analysis without any additional purification. On a Perkin-Elmer 240C elemental analyzer, elemental analysis for carbon, hydrogen and nitrogen, (C, H, N) were performed. A Perkin-Elmer FT-IR spectrum RX1 spectrometer was used to record the infrared (IR) spectra of the materials in KBr (4000–500 cm^{-1}).

Synthesis of CP1

First, 4-avp ligand was synthesized following the literature method.[1] Then, a solution of 4-avp (0.113 g, 0.4 mmol) in MeOH (2 mL) was carefully layered onto $Cd(NO_3)_2 \cdot 4H_2O$ (0.062 g, 0.2 mmol) dissolved in H_2O (2 mL) followed by addition of 2 mL 1:1 (= v/v) solution of MeOH and H_2O. Afterwards, a solution of H_2DCTP (0.047 g, 0.2 mmol) neutralized with Et_3N (0.021 g, 0.2 mmol) in 2 mL EtOH was layered upon it. After few days, yellow coloured block-shaped crystals of [$Cd(DCTP)(4\text{-avp})_2(CH_3OH)_2$] (**1**) were obtained after a week (0.077 g, Yield 45%). Elemental analysis (%) calcd for $C_{52}H_{38}CdCl_2N_2O_6$: C, 64.37; H, 3.95; N, 2.89; found: C, 64.57; H, 4.10; N, 2.79. IR (KBr pellet, cm^{-1}): 1587 $\nu_{as}(COO^{-})$, 1387 $\nu_{sys}(COO^{-})$, 3419 ν(-OH) and fingerprint region (<1500 cm^{-1}).

Synthesis of CP2

CP**2** was prepared in similar way except using H_2DBTP (0.064 g, 0.2 mmol) in stead of H_2DCTP. Yellow coloured block-shaped crystals of [$Cd(DBTP)(4\text{-avp})_2(CH_3OH)(H_2O)$] (**2**)

were obtained after a week (0.094 g, Yield 60%). Elemental analysis (%) calcd for $C_{51}H_{38}Br_2CdN_2O_6$: C, 65.29; H, 5.24; N, 6.62; found: C, 65.09; H, 5.04; N, 6.72. IR (KBr pellet, cm^{-1}): 1602 $\nu_{as}(COO^-)$, 1367 $\nu_{sys}(COO^-)$, 3051 ν(-OH) and fingerprint region (<1500 cm^{-1}).

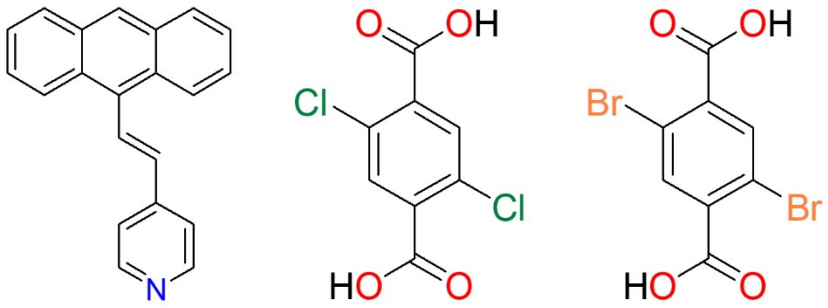

4-avp H_2DCTP H_2DBTP

Scheme S1. Ligands used for the synthesis of CP**1** and CP**2**.

Device fabrication and characterization

Before fabricating the Schottky devices, glass substrates covered with indium tin oxide (ITO) were cleaned using distilled water, acetone and isopropanol in an ultrasonication bath for 20 minutes. Following the preparation of well-dispersed solutions of CP**1** and CP**2** in N,N-dimethylformamide (DMF) medium, the cleaned ITO substrates were spin-coated using a SCU 2700 spin coater running at 600 rpm for one minute. This coating process was carried out four times. The film thickness was measured to be approximately 1 µm after vacuum drying. A HINDHIVAC Vacuum Coating Unit 12A4D was used to deposit aluminium (Al) electrodes onto the films at a pressure of 10^{-6} Torr. A shadow mask was used to define the electrode area, which was 7.065×10^{-6} m^2. Using a Keithley 2635B source meter in a two-probe arrangement, I-V characteristics of the devices containing CP**1** and CP**2** were recorded under dark conditions over a voltage range of -1 V to +1 V at room temperature.

Table S1. Selected bond lengths (Å) in CP**1** and CP**2**

CP**1**	(Å)	CP**2**	(Å)
Cd(1)-O(1)	2.339(3)	Cd(1)-O(1)	2.311(9)
Cd(1)-O(2)	2.288(2)	Cd(1)-O(3)	2.249(7)
Cd(1)-N(1)	2.317(3)	Cd(1)-O(7)	2.329(11)
Cd(1)-$O(1)_a$	2.339(3)	Cd(1)-N(1)	2.332(9)
Cd(1)-$O(2)_a$	2.288(2)	Cd(1)-N(2)	2.320(8)
Cd(1)-$N(1)_a$	2.317(3)	Cd(1)-$O(6)_b$	2.257(6)

Symmetry transformations used to generate equivalent atoms:
a = 1-x, -y, -z; b = -1+x, y, 1+z.

Table S2. Selected bond angles (°) in CP**1**

O(1)-Cd(1)-O(2)	90.94(9)	O(2)-Cd(1)-$N(1)_a$	89.78(10)
O(1)-Cd(1)-N(2)	92.35(10)	$O(1)_a$-Cd(1)-N(1)	87.65(10)
O(1)-Cd(1)-$O(1)_a$	180.00	O(2)-Cd(1)-N(1)	89.78(10)
O(1)-Cd(1)-$O(2)_a$	89.06(9)	N(1)-Cd(1)-$N(1)_a$	180.00
O(1)-Cd(1)-$N(1)_a$	87.65(10)	$O(1)_a$-Cd(1)-$O(2)_a$	90.94(9)
O(2)-Cd(1)-N(1)	90.22(10)	$O(1)_a$-Cd(1)-$N(1)_a$	92.35(10)
$O(1)_a$-Cd(1)-O(2)	89.06(9)	$O(2)_a$-Cd(1)-$N(1)_a$	128.4(3)
O(2)-Cd(1)-$O(2)_a$	180.00		

Symmetry transformations used to generate equivalent atoms: a = 1-x, -y, -z.

Table S3. Selected bond angles (°) in CP**2**

O(1)-Cd(1)-O(3)	90.1(3)	O(3)-Cd(1)-O(6)$_b$	179.1(2)
O(1)-Cd(1)-O(7)	178.1(3)	O(7)-Cd(1)-N(1)	95.3(3)
O(1)-Cd(1)-N(1)	86.3(3)	O(7)-Cd(1)-N(2)	84.9(3)
O(1)-Cd(1)-N(2)	93.5(3)	O(6)$_b$-Cd(1)-O(7)	89.9(3)
O(1)-Cd(1)-O(6)$_b$	89.2(3)	N(1)-Cd(1)-N(2)	178.3(3)
O(3)-Cd(1)-O(7)	90.8(3)	O(6)$_b$-Cd(1)-N(1)	89.7(3)
O(3)-Cd(1)-N(1)	90.8(3)	O(6)$_b$-Cd(1)-N(2)	88.6(3)
O(3)-Cd(1)-N(2)	90.9(3)		

Symmetry transformations used to generate equivalent atoms: b = -1+x, y, 1+z.

Table S4. Hydrogen bonding in CP**2**

D—H···A	Distance (Å) D—H	Distance (Å) H···A	Distance (Å) D··A	Angle (°) ∠D—H···A
O(5)-H(5)……Br(2)	0.8200	2.6400	3.366(9)	149.00
O(5)-H(5)……O(7)	0.8200	2.1600	2.602(13)	114.00

Table S5. Geometric features of π···π stacking interactions in CP**1** and CP**2**.

Compound	**Cg(Ring I)···Cg(Ring J)**	**Cg···Cg (Å)**	**Cg(I)···Perp (Å)**	**Cg(J)···Perp (Å)**
CP**1**	Cg(2)···Cg(2)	3.760(2)	3.5877(15)	3.5877(15)
CP**1**	Cg(2)···Cg(3)	3.845(2)	3.5864(15)	3.6049(17)
CP**1**	Cg(2)···Cg(6)	3.603(2)	3.5989(15)	3.5983(13)
CP**1**	Cg(2)···Cg(8)	3.7713(19)	3.6000(15)	3.5991(11)

CP**1**	Cg(3)···Cg(4)	3.786(2)	3.5901(17)	3.6334(18)
CP**1**	Cg(3)···Cg(7)	3.617(2)	3.6064(17)	3.6112(13)
CP**1**	Cg(3)···Cg(8)	3.857(2)	3.6126(17)	3.5983(11)
CP**1**	Cg(6)···Cg(6)	3.8498(18)	3.6007(13)	3.6006(13)
CP**1**	Cg(6)···Cg(7)	3.7759(18)	3.5949(13)	3.6134(13)
CP**1**	Cg(6)···Cg(8)	3.6158(17)	3.6084(13)	3.6105(11)
CP**1**	Cg(8)···Cg(8)	3.7828(16)	3.6113(11)	3.6113(11)
CP**2**	Cg(1)···Cg(8)	4.052(6)	3.648(5)	3.372(4)
CP**2**	Cg(2)···Cg(8)	4.100(6)	3.695(5)	3.416(4)

Cg(I)···Perp = Perpendicular distance of Cg(I) on ring J. Cg(J)···Perp = Perpendicular distance of Cg(J) on ring I.

For CP**1:**

Cg(2) = Centre of gravity of the ring [C(8)-C(9)-C(14)-C(15)-C(16)-C(17)]

Cg(3) = Centre of gravity of the ring [C(9)-C(10)-C(11)-C(12)-C(13)-C(14)]

Cg(4) = Centre of gravity of the ring [C(16)-C(17)-C(18)-C(19)-C(20)-C(21)]

Cg(6) = Centre of gravity of the ring [C(8)-C(9)-C(10)-C(11)-C(12)-C(13)-C(14)-C(15)]

Cg(7) = Centre of gravity of the ring [C(8)-C(9)-C(14)-C(15)-C(16)-C(21)-C(20)-C(19)]

Cg(8) = Centre of gravity of the ring [C(8)-C(9)-C(10)-C(11)-C(12)-C(13)-C(14)-C(15)]

For CP**2:**

Cg(1) = Centre of gravity of the ring [N(1)-C(1)-C(51)-C(3)-C(4)-C(5)]

Cg(2) = Centre of gravity of the ring [N(2)-C(30)-C(31)-C(32)-C(33)-C(34)]

Cg(8) = Centre of gravity of the ring [C(23)-C(24)-C(25)-C(26)-C(28)-C(29)]

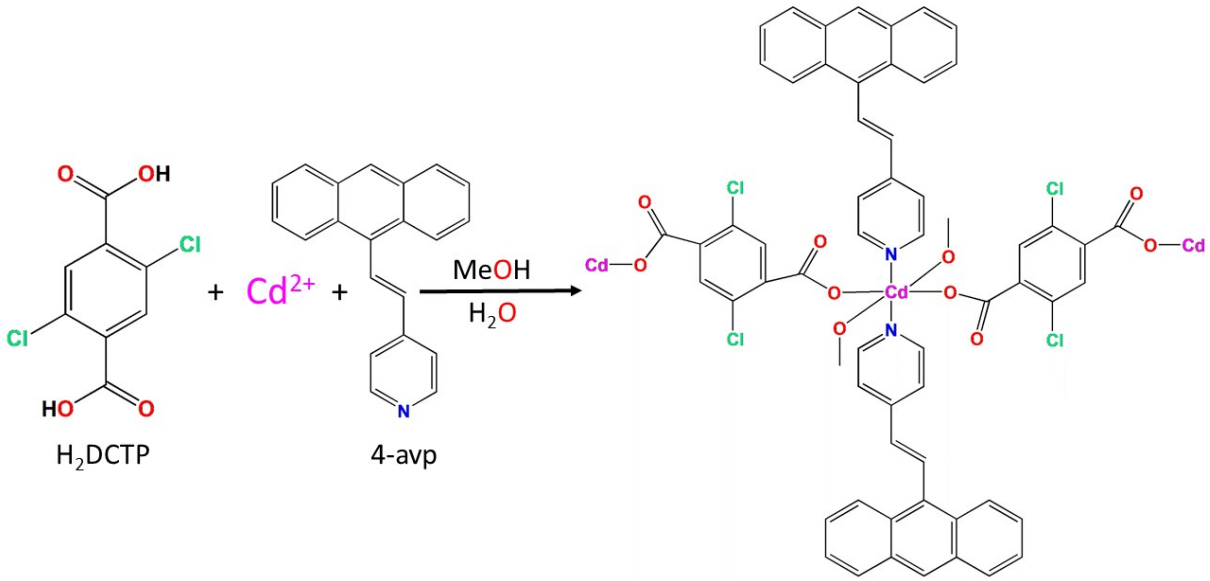

Scheme S2. Synthetic route of CP**1**.

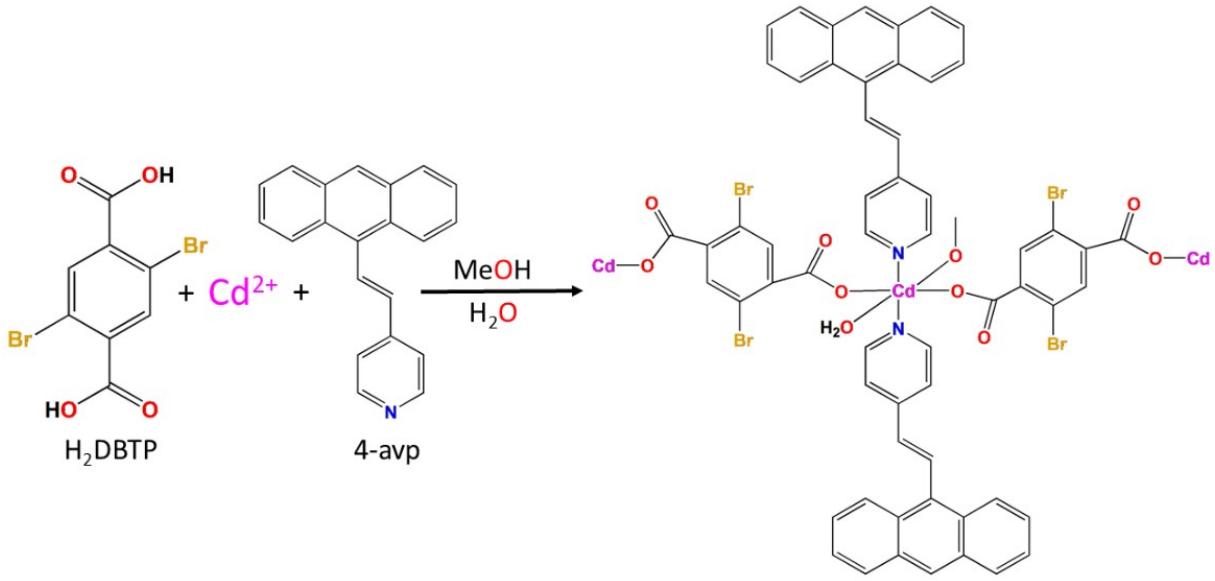

Scheme S3. Synthetic route of CP**2**.

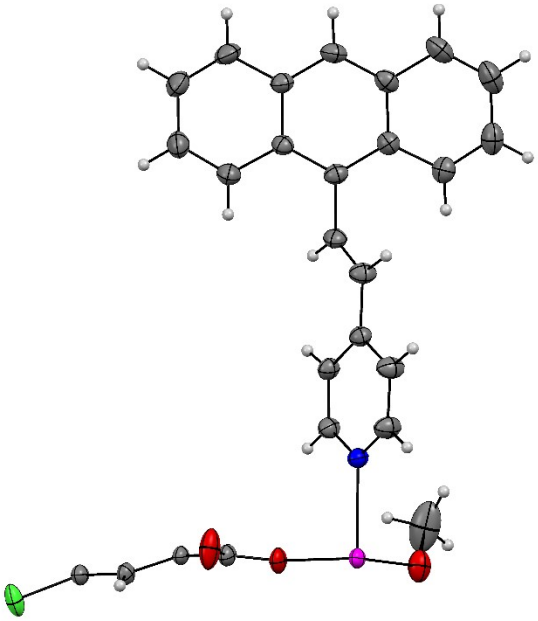

Fig. S1. Asymmetric unit of CP**1** with 30% ellipsoid probability. Color scheme: carbon (gray), oxygen (red), nitrogen (blue), chlorine (green) and Cadmium (magenta).

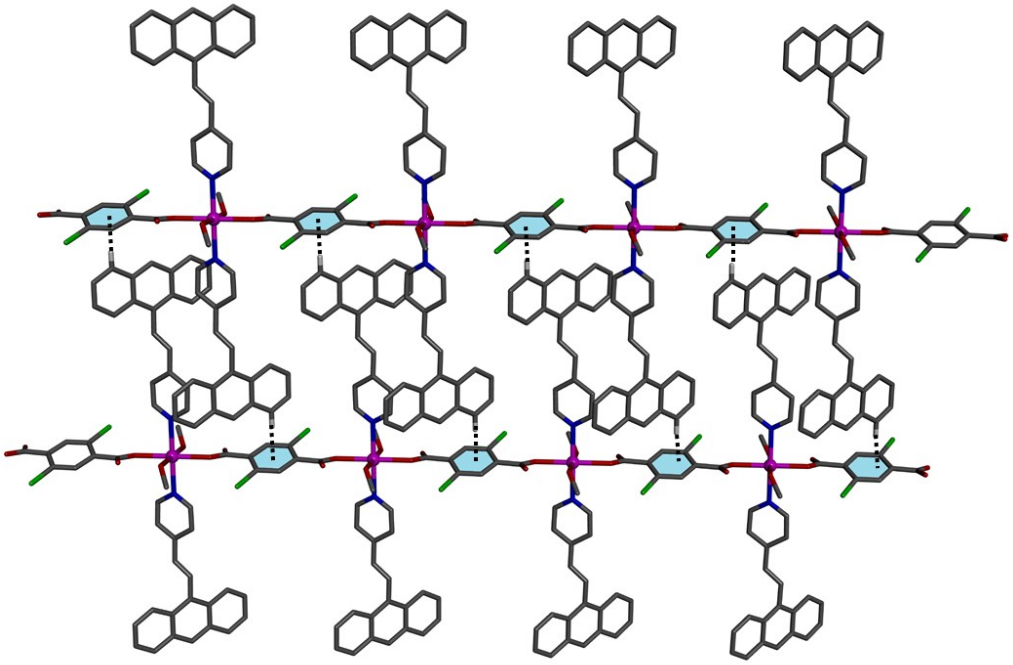

Fig. S2. 2D network formed by C-H··· π interactions in CP**1**. Only selected atoms are shown for the clarity.

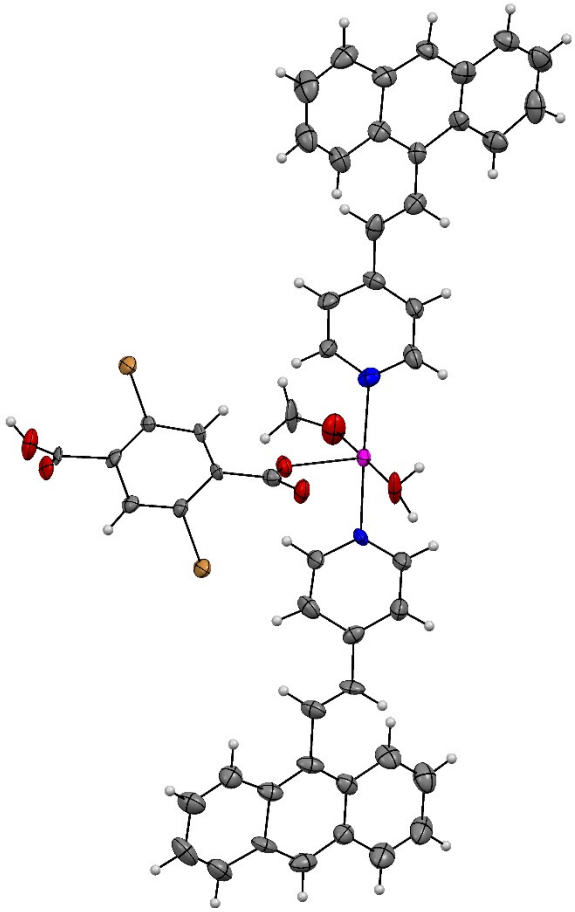

Fig. S3. Asymmetric unit of CP**2** with 30% ellipsoid probability. Color scheme: carbon (gray), oxygen (red), nitrogen (blue), bromine (orange) and Cadmium (magenta).

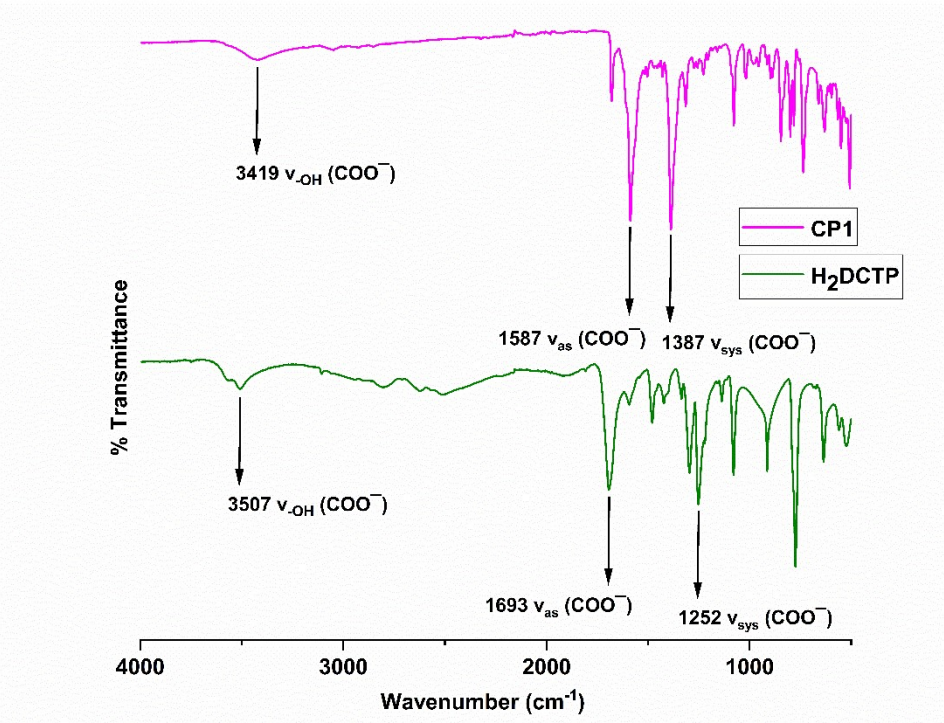

Fig. S4. IR spectrum of 2,5-dichloroterephthalic acid and CP**1** [fingerprint region (<1500 cm^{-1})].

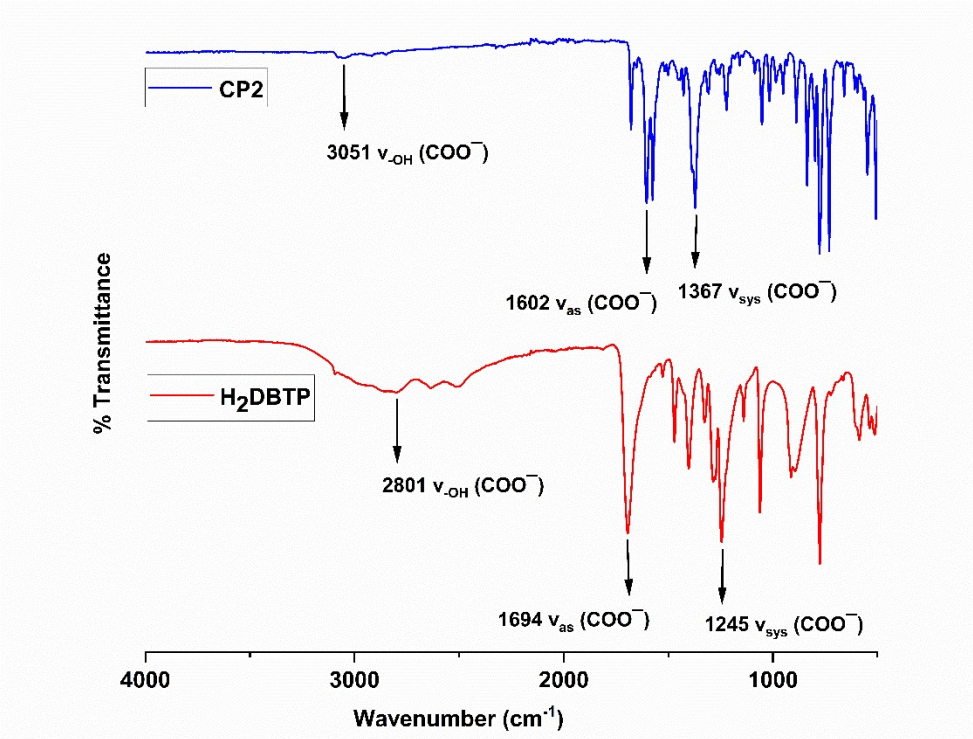

Fig. S5. IR spectrum of 2,5-dibromoterephthalic acid and CP**2** [fingerprint region (<1500 cm^{-1})].

Optical measurements

UV−vis absorption study was conducted at room temperature to investigate the optical properties of the synthesized CPs. The absorption spectra were recorded in the wavelength range of 390−600 nm. Fig. S6 (inset) shows that CP**1** exhibits stronger absorption than CP**2**. Additionally, CP**1** displays a red shift in its optical absorption edge.[2]The band gaps of the CPs were calculated based on Tauc's method using the following equation.[3]

$$(\alpha h\upsilon)^m = A(h\upsilon - E_g) \quad (1)$$

Here, h represents Planck's constant, α is the absorption coefficient, ν is the photon frequency, A is a constant, and m denotes the type of electronic transition (m = 2 for direct transitions and m = 1/2 for indirect transitions). The spectra shown in Fig. S6 present the corresponding Tauc plots for the synthesized CPs. The optical band gaps were determined by extrapolating the linear region of the plot to the energy axis. The intercepts yield band gap values of 2.22 eV for CP**1** and 2.27 eV for CP**2**. These results indicate that both synthesized CPs possess intrinsic semiconducting properties. However, CP**1** has a slightly higher absorption capability and a marginally lower band gap compared to CP**2**.

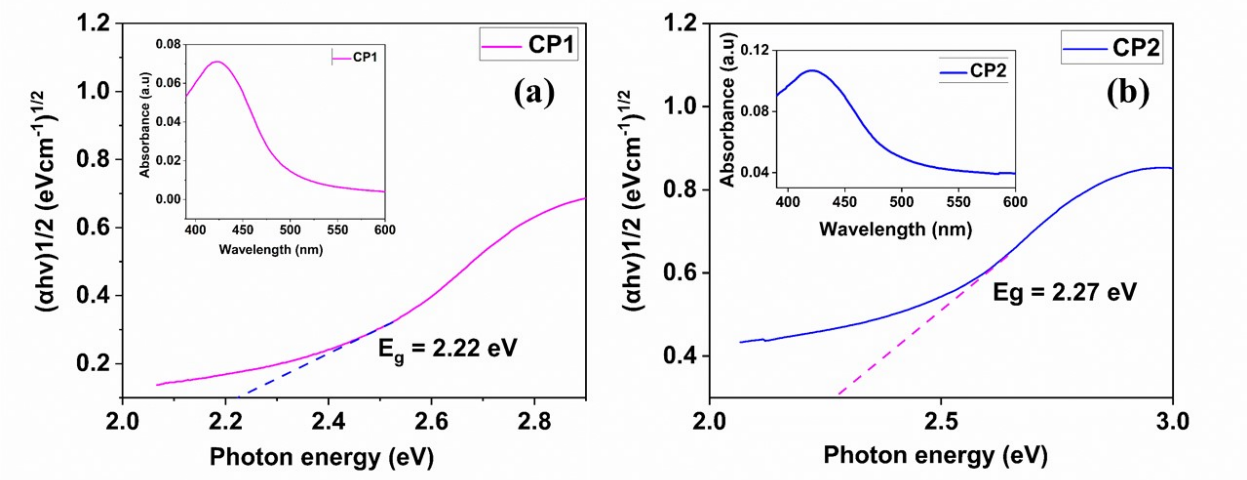

Fig. S6. (a) UV-Vis absorption (inset) and Tauc's plot of (a) CP**1** and (b) CP**2**.

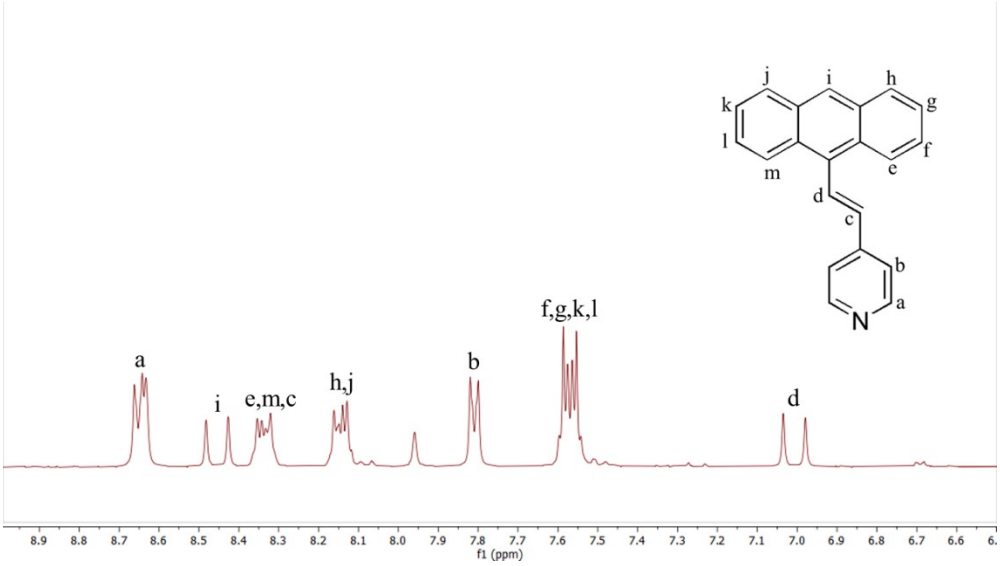

Fig. S7. Partial ^{1}H NMR spectra (400 MHz, DMSO-d_6) of CP**1**.

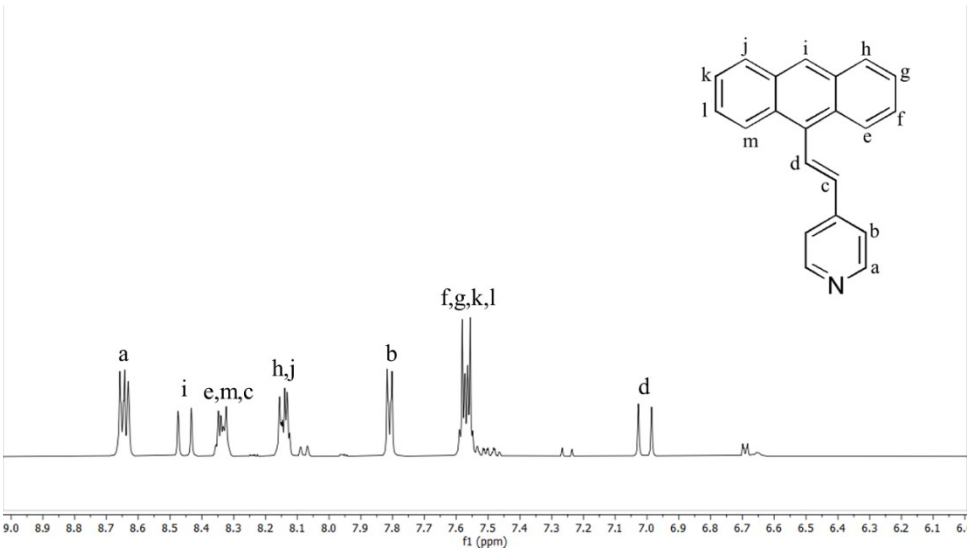

Fig. S8. Partial ^{1}H NMR spectra (400 MHz, DMSO-d_6) of CP**2**.

Hirshfeld analysis

Utilizing the Crystal Explorer programme 17.5,[4] intermolecular and intramolecular interactions have been estimated for the crystalline and molecular structures over the Hirshfeld surface. The study considers the area around the molecule in the crystal space that compares the inner reference molecule from the outer neighbouring molecule.[5] The comparisons are measured with various attributes, such as d_{norm}, electrostatic potential, shape index, and curvature named Hirshfeld surface.[6,7] The measurement results provided by Hirshfeld Surfaces are accountable to quantify intermolecular interactions in the form of a graphical percentage representation i.e. fingerprint plots which further provide more valuable information about the crystal packing.[8,9] The Hirshfeld surface d_{norm} is plotted around the asymmetric unit by means of the normalized contact distance surface. Valuable insights into the intermolecular contacts and associations can be obtained by investigating the interactions inside the asymmetric unit that contributes to the overall crystal packing.[10] The d_{norm} property is a symmetric function of the surface distances among the nuclei inside and outside (d_i and d_e, respectively) for target elements relative to van der Waals radius. The reference red and blue areas in d_{norm} reflect shorter and longer interconnects, and the white color indicates contact around the van der Waals radius.[11] Two-dimensional (2D) fingerprint plots convert extent of interaction into a percentage to provide more relevant facts regarding intramolecular contact within a crystal.[12,13] There by, Hirshfeld surface analysis is a useful tool in describing the nature of intramolecular interactions that affect molecular packing in crystals.

Hirshfeld surface analysis of CP1

Hirshfeld Surface analysis is a useful and popular technique that offers a quantitative analysis

of strong and weak contacts amongst atoms or residues in a crystal packing. The smallest repeating unit of CP**1** consists of one Cd(II) centre, one avp [4-[2-(9-anthryl)vinyl] pyridine)], and half 2,5-dichloroterephthalate (H_2DCTP) linkers and one methanol representing the asymmetric unit of the crystal, which is chosen as the basic fragment for Hirshfeld analysis. The resulting surfaces include d_{norm}, shape index, and curvedness (Fig. S9) associated with the essential features of the crystal structure. The asymmetric unit has been analyzed to study the Hirshfeld surfaces which include d_{norm}, shape index, and curvedness (Fig. S9). In order to support the observer to understand the calculations by considering the view of the surrounding structural atmosphere, one of the representations (d_{norm}) is made in transparent mode. The leading interaction was discovered between C and H atoms for CP**1**.

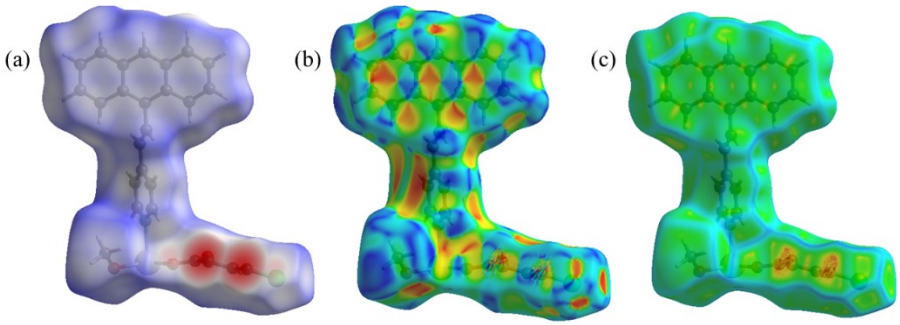

Fig. S9. Hirshfeld surfaces mapped over (a) d_{norm} (b) shape index and (c) curvedness for CP**1**.

The color scheme in d_{norm} includes red patches in Fig. S9a, mainly correspond to the neighboring H···O contacts consequential from C-H···O hydrogen bonds. Similarly, unique features of the crystal surface namely curvature have been introduced in terms of shape index (Fig. S9b) and curvedness parameters (Fig. S9c) to offer more chemical insight into the

crystal structure. The shape index includes a combination of adjacent red and blue patterns, revealing the presence of aromatic stacking interactions (C-H···π). Curvedness maps typically represent large regions of green comparatively flat separated via blue edges having prominent curvedness indicating the presence of π···π stacking interactions. The 2D diagrams are represented in the form of small plots with green-blue color on their surfaces, specifying particular atomic interactions such as O···H or C···H in CP**1**. The combined contribution of all these interactions is displayed in the full fingerprint plot (Fig. S10). The extent of H··C/C··H interactions include 26.5% of the total surface of CP**1**. The upper sharp point (d_i =1.12, d_e = 1.6 Å) represents the interactions of H··C, and correspondingly, the lower sharp point (d_i = 1.6, d_e = 1.12 Å) represents the interactions of C··H on the d_{norm} surface. On the other hand, the magnitude of interactions between O··H/H··O was found 10.7%. The upper sharp point (d_i = 1.15, d_e = 1.40 Å) represents the interaction of H··O, and correspondingly, the lower sharp point (d_i = 1.40, d_e = 1.15 Å) shows the interaction of O···H. On the other hand, the magnitude of interactions between Cl··H/H··Cl was found 9%. The upper sharp point (d_i = 1.15, d_e = 1.7 Å) represents the interaction of H··Cl, and correspondingly, the lower sharp point (d_i = 1.7, d_e = 1.15 Å) shows the interaction of Cl···H. These can be observed from the bright red spots displayed on the d_{norm} surface (Fig. S9) and strong non-covalent interactions further facilitate the overall packing stability of the crystal.

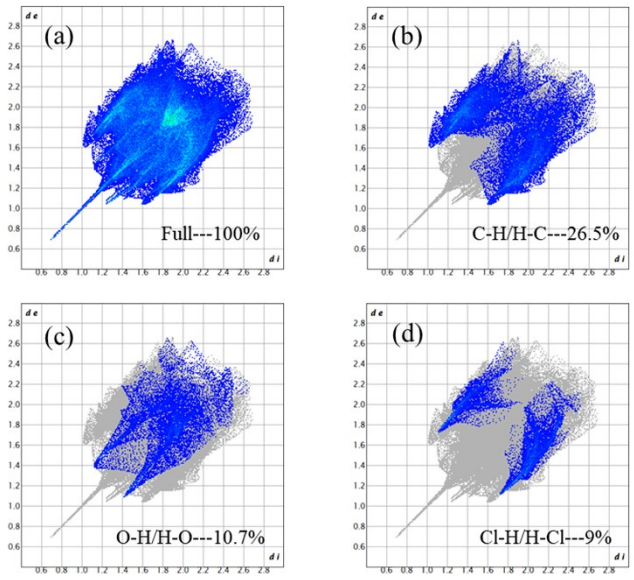

Fig. S10. 2D fingerprint plots: (a) Full (b) C···H/H···C (c) O···H/H···O (d) Cl···H/H···Cl.

Hirshfeld surface analysis of CP2

Hirshfeld Surface analysis is a useful and popular technique that offers a quantitative analysis of strong and weak contacts amongst atoms or residues in a crystal packing. The smallest repeating unit of CP**2** consists of one Cd(II) centre, two avp [4-[2-(9-anthryl)vinyl] pyridine)], and one 2,5-dibromoterephthalate (H_2DBTP) linkers and one water molecule and one methanol molecule representing the asymmetric unit of the crystal, which is chosen as the basic fragment for Hirshfeld analysis. The resulting surfaces include d_{norm}, shape index, and curvedness (Fig. S11) associated with the essential features of the crystal structure. The asymmetric unit has been analyzed to study the Hirshfeld surfaces which include d_{norm}, shape index, and curvedness (Fig. S11). In order to support the observer to understand the calculations by considering the view of the surrounding structural atmosphere, one of the representations (d_{norm}) is made in transparent mode. The leading interaction was discovered between C and H atoms for CP**2**.

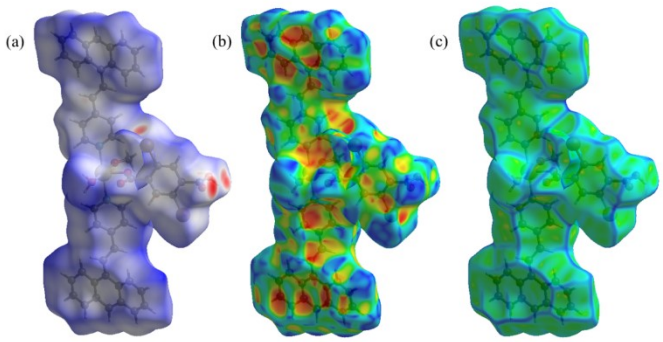

Fig. S11. Hirshfeld surfaces mapped over (a) d_{norm} (b) shape index and (c) curvedness for CP**2**.

The color scheme in dnorm includes red patches in Fig. S11a, mainly correspond to the neighboring H···O contacts consequential from C-H···O hydrogen bonds. Similarly, unique features of the crystal surface namely curvature have been introduced in terms of shape index (Fig. S11b) and curvedness parameters (Fig. S11c) to offer more chemical insight into the crystal structure. The shape index includes a combination of adjacent red and blue patterns, revealing the presence of aromatic stacking interactions (C-H···π). Curvedness maps typically represent large regions of green comparatively flat separated via blue edges having prominent curvedness indicating the presence of π···π stacking interactions. The 2D diagrams are represented in the form of small plots with green-blue color on their surfaces, specifying particular atomic interactions such as O···H, C···H and Br···H in CP**2**. The combined contribution of all these interactions is displayed in the full fingerprint plot (Fig. S12). The extent of H··C/C··H interactions include 29.7% of the total surface of CP**2**. The upper sharp point (di =1.65, de = 1.15 Å) represents the interactions of H··C, and correspondingly, the lower sharp point (di = 1.15, de = 1.65 Å) represents the interactions of C··H on the dnorm surface. On the other hand, the magnitude of interactions between O··H/H··O was found 10.3%. The upper sharp point (di = 0.9, de = 1.2 Å) represents the interaction of H··O, and

correspondingly, the lower sharp point (di = 1.2, de = 0.9 Å) shows the interaction of O···H. On the other hand, the magnitude of interactions between Br··H/H··Br was found 6%. The upper sharp point (di = 0.9, de = 1.6 Å) represents the interaction of H··Br, and correspondingly, the lower sharp point (di = 1.6, de = 0.9 Å) shows the interaction of Br···H. These can be observed from the bright red spots displayed on the d_{norm} surface (Fig. S11) and strong non-covalent interactions further facilitate the overall packing stability of the crystal.

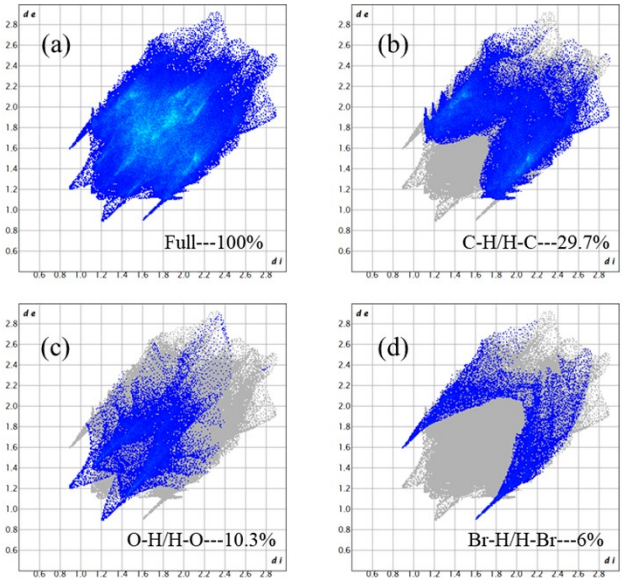

Fig. S12. 2D fingerprint plots: (a) Full (b) C···H/H···C (c) O···H/H···O (d) Br···H/H···Br.

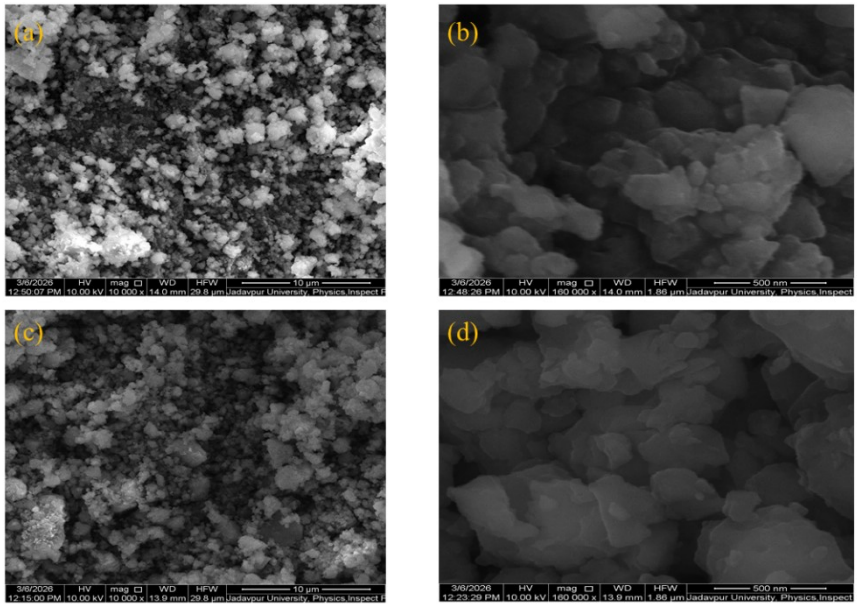

Figure S13. FESEM micrographs of (a, b) CP**1** and (c, d) CP**2** in different magnification.

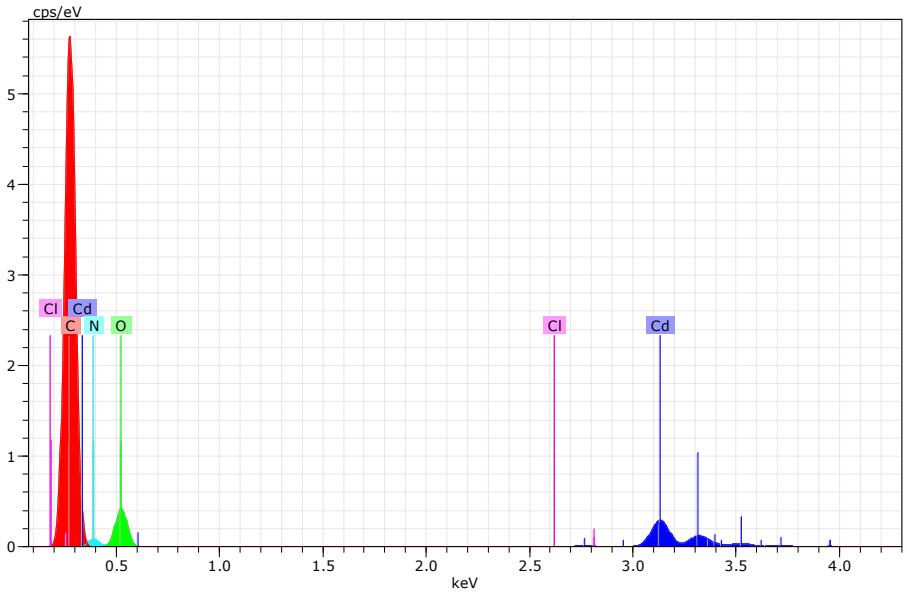

Fig. S14. EDX spectra corresponding weight percentage and atomic percentage table for CP**1**.

Element	unn. C [wt.%]	norm. C [wt.%]	Atom. C [at.%]	Compound norm. [wt.%]	Comp. C Error (3 Sigma) [wt.%]
Carbon	71.71	71.71	77.80	71.71	29.99
Oxygen	18.34	18.34	14.94	18.34	13.15
Cadmium	2.45	2.45	0.28	2.45	0.39
Nitrogen	7.50	7.50	6.98	7.50	9.64
Total:	100.00	100.00	100.00		

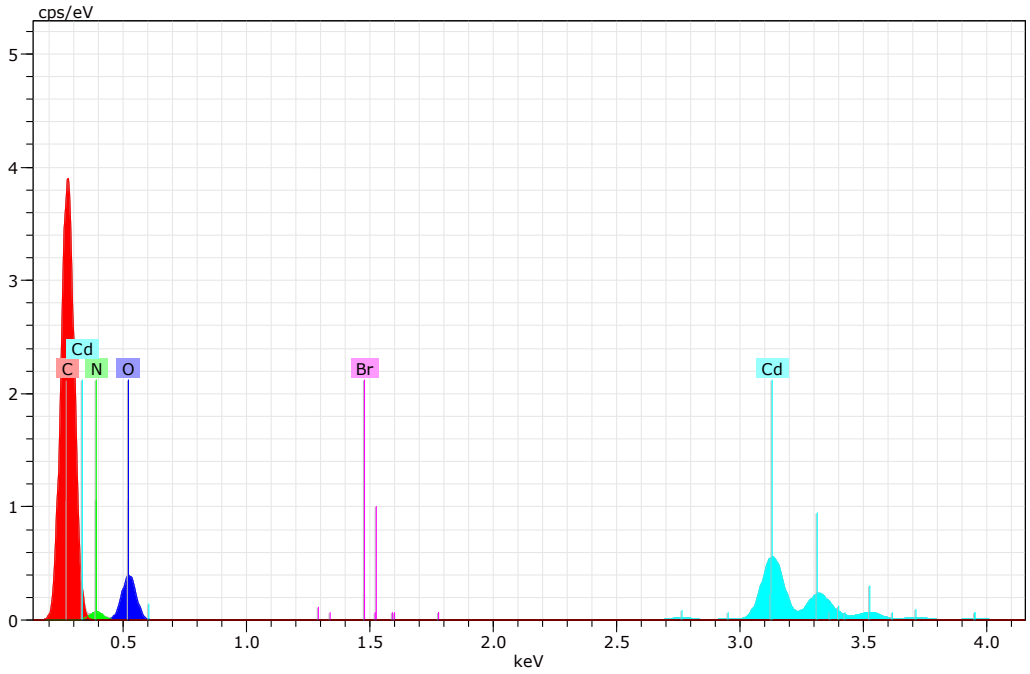

Fig. S15. EDX spectra corresponding weight percentage and atomic percentage table for CP**2**.

Element	unn. C [wt.%]	norm. C [wt.%]	Atom. C [at.%]	Compound norm. [wt.%]	Comp. C Error (3 Sigma) [wt.%]
Carbon	64.80	64.80	73.53	64.80	27.92
Nitrogen	8.10	8.10	7.88	8.10	10.03
Oxygen	20.94	20.94	17.84	20.94	14.59
Cadmium	6.16	6.16	0.75	6.16	0.76
Bromine	0.00	0.00	0.00	0.00	0.00
Total:	100.00	100.00	100.00		

Table S6. Previously reported conductivity properties of CPs

Sl. No	Compounds	Structures	Structural features	Conductivity ($S\ m^{-1}$)	Ref
1.	$\{[Cd_2(1,4\text{-}(2\text{-Me})\text{-bix})(msuc)]\cdot(H_2O)\}_n$ [1,4-(2-Me)-bix=1,4-bis[(2-methyl-1-imidazolyl)-methyl]benzene and msuc = disodiummethyl succinate]	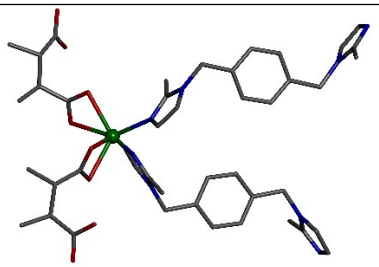	2D CP	1.98×10^{-6}	14
2.	$\{[Cd(HAIPA)(tppz)(OH)]\cdot 3H_2O\}_n$[tppz = 2,3,5,6-tetrakis(2-pyridyl)pyrazine and HAIPA = 5-aminoisophthalate]	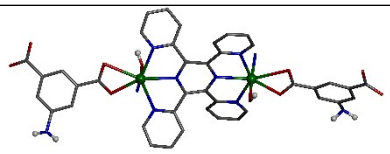	2D CP	7.42×10^{-5}	15
3.	$\{[Cd_2L(IPA)]_2\cdot(CH_3OH)\}_n$ [H_2L = (N,N′-bis(3-methoxysalicylidene)-diethylenetriamine) and IPA = isophthalic acid]	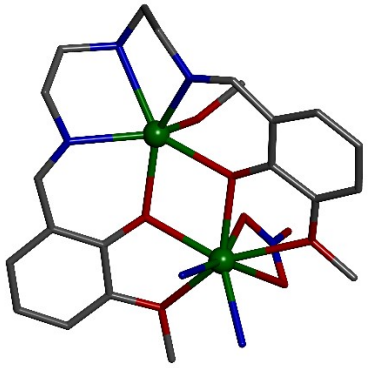	1D CP	5.4×10^{-8}	16
4.	[Cd(nip)(4-Clpy)(CH_3OH)] [H_2nip = 5-nitroisophthalic acid, 4-Clpy = 4-chloropyridine]	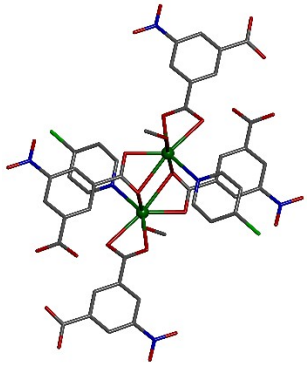	1D CP	12.68×10^{-4}	17

5.	{[$Cd_2I_2(BDC)_2(INH)_2$]·(2DMF)(H_2O)}$_n$ [INH = isoniazid, H_2BDC = terephthalic acid and DMF = dimethylformamide]	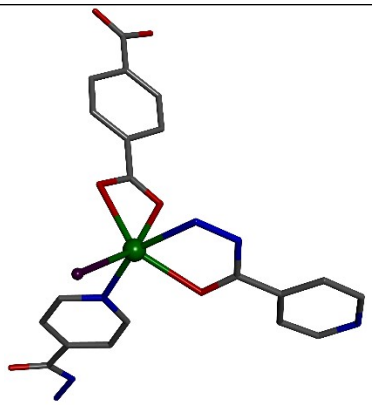	Honeycomb type 2D	5.14×10^{-4}	18
6.	[Cd(4-avp)(5-nip).CH_3OH] [avp = 4-[2-(9-anthryl)vinyl] pyridine) and $H_2$5-nip = 5-nitroisophthalic acid]	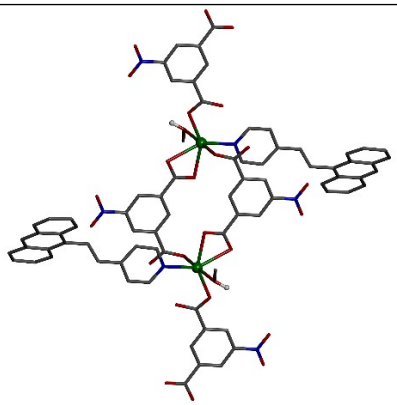	1D ribbon chain	6.33×10^{-4}	19
7.	{[Cd(5-NIP)$_2$(INH)$_2$]·(DMF)$_2$(H_2O)]}$_n$ [$H_2$5-NIP = 5-nitro-isophthalic acid and INH = isonicotinic hydrazide]	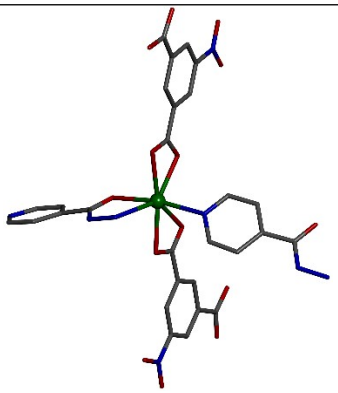	2D CP	5.04×10^{-4}	20
8.	[{Cd_2(cis-1,4-chdc)$_2$(1,10-phen)$_2$}·5H_2O]$_n$ [1,4-H_2chdc = 1,4-cyclohexanedicarboxylic acid and 1,10-phen = 1,10-phenanthroline]	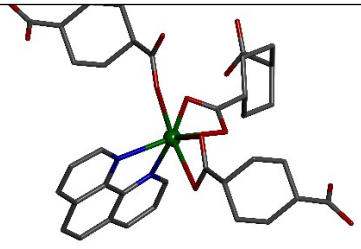	2D CP	7.51×10^{-4}	21

9.	$[Cd(DCTP)(4\text{-}avp)_2]_n$ [4-avp = 4-[2-(9-anthryl)vinyl] pyridine) and H_2DCTP = 2,5-dichloroterephthalic acid]	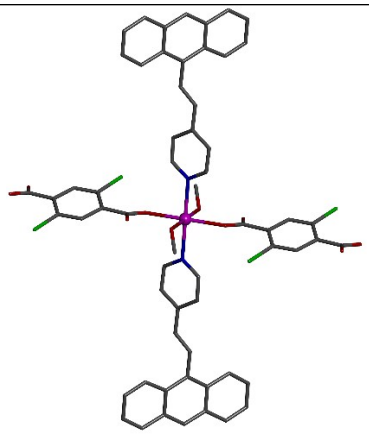	1D CP	7.55×10^{-4}	**This work**
10.	$[Cd(DBTP)(4\text{-}avp)_2]_n$ [4-avp = 4-[2-(9-anthryl)vinyl] pyridine), and H_2DBTP = 2,5 ibromoterephthalic acid]	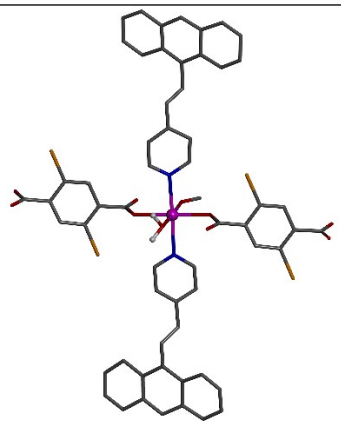	1D CP	3.78×10^{-4}	**This work**

Table S7. Previously reported conductivity parameters of CPs.

Sl. No	**Compounds**	**Material/System**	**Conductivity (Sm^{-1})**	**Ideality Factor (η)**	**Barrier Height (ϕ_b eV)**	**Ref**
1.	[Cd (L)(NA)(H_2O)] [L = Iminol form of N-nicotinoyl glycinate and NA = nicotinate]	Cd-based 2D CP	-	1.24	0.86	22
2.	$[Cd_2(adp)_2(4\text{-}nvp)_4(H_2O)]\cdot(H_2O)_7$ (CP**1**) and $[Zn_2(adp)(4\text{-}nvp)_2(H_2O)(\mu_3\text{-}OH)]\cdot(H_2O)\cdot(NO_3)$ (CP**2**)	Cd(II) 2D CP vs Zn(II) 1D CP	Higher for Cd-CP	0.73 (CP**1**) and 0.58 (CP**2**)	0.56 (CP**1**) and 0.62 (CP**2**)	23

	[H_2adp = adipic acid and 4-nvp = 4-(1 naphthylvinyl)pyridine]					
3.	[Cd(DCTP)(4-avp)$_2$]$_n$ (CP**1**) and [Cd(DBTP)(4-avp)$_2$]$_n$ (CP**2**) [4-avp = 4-[2-(9-anthryl)vinyl] pyridine) and H_2DCTP = 2,5-dichloroterephthalic acid and H_2DBTP = 2,5-dibromoterephthalic acid]	Cd metal ion-based CPs (CP**1** and CP**2**)	Higher for CP**1**	1.07 (CP**1**) and 1.15 (CP**2**)	0.63 (CP**1**) and 0.65 (CP**2**)	**Present Work**

References

1. C. W. Chan, T. F. Lai, C. M. Che and S. M. Peng, *J. Am. Chem. Soc.,* 1993, **115**, 11245-11253.
2. N. Bouazizi, R. Bargougui, A. Oueslati and R. Benslama, *Adv. Mater. Lett.,* 2015, **6**, 158-164.
3. J. Tauc, *Mater. Res. Bull.,* 1968, **3**, 37-46.
4. S. K. Wolff, D. J. Grimwood, J. J. McKinnon, D. Jayatilaka and M. A. Spackman, Crystal Explorer 2.0; University of Western Australia: Perth, Australia, 2007.
5. F. L. Hirshfeld, *Theor. Chim. Acta*., 1977, **44**, 129–138.
6. H. F. Clausen, M. S. Chevallier, M. A. Spackman and B. B. Iversen, *New J. Chem*., 2010, **34**, 193–199.
7. A. L. Rohl, M. Moret, W. Kaminsky, K. Claborn, J. J. McKinnon and B. Kahr, *Cryst. Growth Des.*, 2008, **8**, 4517–4525.

8. A. Parkin, G. Barr, W. Dong, C. J. Gilmore, D. Jayatilaka, J. J. McKinnon, A. M. Spackman and C. C. Wilson, *CrystEngComm*., 2007, **9**, 648–652.
9. M. A. Spackman and J. J. McKinnon, *CrystEngComm*., 2002, **4**, 378–392.
10. H. F. Clausen, M. S. Chevallier, M. A. Spackman and B. B. Iversen, *New J. Chem*., 2010, **34**, 193–199.
11. M. A. Spackman and D. Jayatilaka, *CrystEngComm*., 2009, **11**, 19–32.
12. F. H. Allen, O. Kennard, D. G. Watson, L. Brammer, A. G. Orpen and R. Taylor, *J. Chem. Soc. Perkin Trans.,* 1987, **2**, S1–S19.
13. J. J. McKinnon, M. A. Spackman and A. S. Mitchell, *Acta Cryst*. *B.,* 2004, **60**, 627– 668.
14. S. Ghosh, M. Das, S. Dinda, G. Pahari, P. P. Ray, and D. Ghoshal, *Cryst. Growth Des.,* 2021, **21**, 4892-4903.
15. S. Bhunia, D. Sahoo, S. Maity, B. Dutta, S. Bera, N. B. Manik and C. Sinha, *Inorg. Chem.,* 2023, **62**, 11976-11989.
16. T. K. Ghosh, S. Jana, S. Jana and A. Ghosh, *New J. Chem.,* 2020, **44**, 14733-14743.
17. B. Dutta, A. Dey, C. Sinha, P. P. Ray and M. H. Mir, *Dalton Trans.,* 2019, **48**, 11259-11267.
18. K. Naskar, A. Dey, S. Maity, M. K. Bhunia, P. P. Ray and C. Sinha, *Cryst. Growth Des.,* 2019, **19**, 2206-2218.
19. E. Hossain, R. Sk, M. Das, J. Goura, S. Roy, P. P. Ray, M. H. Mir and S. Mukhopadhyay, *Eur. J. Inorg. Chem*., 2024, **27**, e202300736.
20. K. Naskar, A. Dey, S. Maity, P. P. Ray and C. Sinha, *Cryst. Growth Des*., 2021, **21**, 4847-4856.

21. B. Pal, S. Khan, B. Dutta, S. Naaz, S. Maity, P. Ghosh and M. H. Mir, *CrystEngComm.,* 2021, **23**, 7525-7533.

22. C. Das, V. D. Patel, D. Gupta, P. Mahata, *Inorg. Chem.,* 2024, **63**, 3656-3666.

23. M. Shit, P. Das, A. Samanta, B. Dutta, M. Das, S. Roy, C. Sinha, P. P. Ray and M. H. Mir, *CrystEngComm.,* 2024, **26**, 6618-6626.